Three-phase equilibria of hydrates from computer simulation. III. Effect of dispersive interactions in the methane and carbon dioxide hydrates

J. Algaba[†],[1] S. Blazquez[†],[2] J. M. Míguez,[1] M. M. Conde[*],[3] and F. J. Blas[*1]

[1)] *Laboratorio de Simulación Molecular y Química Computacional, CIQSO-Centro de Investigación en Química Sostenible and Departamento de Ciencias Integradas, Universidad de Huelva, 21006 Huelva Spain*

[2)] *Dpto. Química Física I, Fac. Ciencias Químicas, Universidad Complutense de Madrid, 28040 Madrid, Spain*

[3)] *Departamento de Ingeniería Química Industrial y del Medio Ambiente, Escuela Técnica Superior de Ingenieros Industriales, Universidad Politécnica de Madrid, 28006, Madrid, Spain.*

In this work, the effect of the range of the dispersive interactions in the determination of the three-phase coexistence line of the CO_2 and CH_4 hydrates has been studied. In particular, the temperature (T_3) at which solid hydrate, water, and liquid CO_2/gas CH_4 coexist has been determined through molecular dynamics simulations using different cut-off values (from 0.9 to 1.6 nm) for the dispersive interactions. The T_3 of both hydrates has been determined using the direct coexistence simulation technique. Following this method, the three phases in equilibrium are put together in the same simulation box, the pressure is fixed, and simulations are performed at different temperatures T. If the hydrate melts, then $T > T_3$. Contrary, if the hydrate grows, then $T < T_3$. The effect of the cut-off distance on the dissociation temperature has been analyzed at three different pressures for CO_2 hydrate, namely, 100, 400, and 1000 bar. Then, we have changed the guest and studied the effect of the cut-off distance on the dissociation temperature of the CH_4 hydrate at 400 bar. Also, the effect of long-range corrections for dispersive interactions has been analyzed by running simulations with homo- and inhomogeneous corrections and a cut-off value of 0.9 nm. The results obtained in this work highlight that the cut-off distance for the dispersive interactions affects the stability conditions of these hydrates. This effect is enhanced when the pressure is decreased, displacing the T_3 about $2-4$ K depending on the system and the pressure.

[*]Corresponding authors: felipe@uhu.es and maria.mconde@upm.es

[†]These authors contributed equally to this work

I. INTRODUCTION

Clathrate hydrates are non-stochiometric crystalline inclusion compounds consisting of a network of hydrogen-bonded molecules (host) conforming cages in which small molecules (guest) can be encapsulated under the appropriate thermodynamic conditions. When the host molecule is water, these compounds are simply called hydrates.[1] The structure of the hydrates depends on the thermodynamic conditions, but moreover, depends on the guest molecule encapsulated inside the hydrate. The guest has a high impact on the stability of the hydrate. Hydrates of small molecules, such as methane (CH_4) or carbon dioxide (CO_2), often crystallize forming the so-called structure sI. Hydrates of medium molecules (i.e., butane, cyclopentane, or tetrahydrofuran) crystallize in structure sII,[1] although this structure is also stabilized by very small guests such as N_2 and H_2.[2] Finally, when there is a mixture of large and small molecules the sH structure is the most common.[1]

Due to the capability of hydrates to store CH_4[3,4] and other low molecular weight hydrocarbons, hydrates are potential sources of natural gas and, therefore, energy. One of the greatest challenges of society is the high energy demand. The fact that the world is constantly evolving towards a more technological society means that energy demand is increasing. Although it is true that more renewable and/or alternative energy sources are being used, in 2022 the main source of energy was fossil fuels (more than 62% of the electricity generated in the world).[5] It is estimated that the amount of natural gas stored in hydrates far exceeds the amount of natural gas available from conventional sources. Other interesting applications of hydrates from a social, environmental, and industrial point of view is their capability to sequester CO_2,[6–8] as well as to store and transport gases, being especially interesting in the case of hydrogen (H_2).[9–18] Another relevant aspect in the study of hydrates is the use of additives. The thermodynamic stability conditions of these compounds can be highly modified by the use of additives, also known as hydrate promoters/inhibitors.[19–34] Thermodynamic hydrate promoters are additives that will allow hydrate formation under conditions where it would not normally exist (higher temperatures and lower pressures). Contrarily, the use of inhibitors prevents the formation of these compounds.

The thermodynamics of hydrates has been studied experimentally,[1,35–41] theoretically,[42,43] and by molecular simulation.[44–51] Thus, the stability conditions of these compounds are well established. Molecular simulation has the advantage of studying these systems from a microscopic perspective, given information about not only the thermodynamics, including phase equilibria, and structure but also the dynamic of the growing/melting of these compounds. However, molecular simulation studies have to be performed carefully due to a series of approximations/limitations that have to be taken into account.[52,53] One of the most important limitations is the size of the system that can be simulated. Realistic systems, with an Avogadro number order of molecules, are out of the possibilities of the current supercomputers. Typically, the size of the systems studied through molecular dynamic (MD) or Monte Carlo (MC) simulations goes from a few molecules to $\sim 10^5$. This manuscript is the third part of a series of papers

devoted to investigate the effects of finite-size and dispersion interactions on the three-phase equilibria of CH_4 and CO_2 hydrates from computer simulation. For a detailed analysis of the finite-size effect on the dissociation temperatures of CO_2 and CH_4 hydrates, we recommend the reader the two first papers of the series.[54,55]

To keep the system in a condensed phase and prevent the molecules to escape from the simulation box, it is necessary to use a potential that works in the same way as a container (boundary conditions). In order to avoid the so-called border effects, that take place when the molecules "feel" the border of the simulation box, periodic boundary conditions (PBC) are used routinely in simulation.[52,53] This technique implies to replicate the simulation box in the space. The real simulation box is in the middle of a network conformed by identical images of the original simulation box. If one molecule escapes through one side of the box, the same molecule enters from the opposite side of the box, from one of the replicated images. The PBC technique allows to keep constant the number of molecules inside the simulation box avoiding border effects with non-extra computational effort. As a consequence of the infinite number of replicated boxes, two considerations have to be taken into account. The first one is that a molecule is going to interact only with the closest molecule image among all the possible replicated simulation boxes (minima image criteria). The second one is that to avoid the interaction of a molecule with itself in one of the replicated boxes, the interaction range or cut-off distance, r_c, cannot be larger than half of the shortest side of the simulation box.

The election of the cut-off distance plays a key role in molecular simulation. Its value governs the range of the interactions between the molecules forming the system under study. Two chemical groups of the same or different molecules will interact if the separation between them is smaller than r_c. In other words, the interactions between chemical groups separated further than the cut-off distance are neglected. Since its value impacts on the determination of the energy of the system, all the thermodynamic, structural, and dynamical properties could be hardly affected by its particular election. The larger the value of r_c, the better the accuracy of the calculated properties associated with the full intermolecular potential.

The use of high cut-off values in simulations entails large computational efforts. According to this, it is necessary to find a compromise between accuracy and the CPU time needed in the calculations. Typically, the cut-off distances used in the literature to study hydrates range from 0.9 to 1.1 nm.[44–50] Very recently, some of us have analyzed the effect of r_c on the three-phase coexistence temperature, T_3, at a given pressure of the CO_2 and CH_4 hydrates from computer simulation.[47,56] As far as we know, these works are the only studies in the literature that consider the effect of the cut-off distance on the T_3 of hydrates. Particularly, the dissociation temperatures, at 400 bar, have been determined using $r_c = 1.0$ and 1.9 nm, for the case of the CO_2 hydrate, and $r_c = 0.9$ and 1.7 nm for the CH_4 hydrate. The effect of changing the cut-off distance is small but not negligible: T_3 increases from 290 to 292 K in the case of the CO_2 hydrate, and decreases from 297 to 295 K in the case of the CH_4 hydrate.

The goal of this work is to understand, from a molecular perspective, the effect of the cut-off distance of the dispersive interactions on the dissociation temperature of hydrates. To this end, we combine molecular dynamics simulations and the well-known direct coexistence technique to determine the T_3 values, at several pressures, of the CO_2 and CH_4 hydrates using different cut-off values. We also perform additional independent simulations to assess the effect of using homogeneous and inhomogeneous long-range corrections on the dispersive interactions on the dissociation temperatures of both hydrates.

The rest of the paper is organized as follows: In Sec. II, we describe the simulation details and the molecular models used in this work. In Sec. III we describe the methodology used to analyze the effect of the cut-off on the T_3 at different pressures of the CO_2 and CH_4 hydrates. The results obtained, as well as their discussion, are described in Sec. IV. Finally, conclusions are presented in Sec. V

II. SIMULATION DETAILS AND MOLECULAR MODELS

A. Simulation details

MD simulations are carried out through the GROMACS package.[57] Here it is important to mention that all simulations have been carried out using GROMACS version 4.6 in double precision except for simulations where the particle mesh Ewalds long-range corrections[58,59] for the dispersive interactions have been taking into account. GROMACS version 4.6 doesn't support this long-range correction, and for this reason, simulations have been performed using the version 2016 in double precision. In all cases, the simulations are run using the *NPT* or isothermal-isobaric ensemble, allowing each side of the simulation box to change independently to keep the pressure constant as well as to avoid any stress from the hydrate solid structure. We use the Verlet-leapfrog[60] algorithm for solving Newton's equations of motion with a time step of 2 fs. In order to keep the temperature and the pressure constant along the simulation, the Nosé-Hoover thermostat[61] and the anisotropic Parrinello-Rahman barostat[62] are used with a time constant of 2 ps. In the case of the Parrinello-Rahman barostat, a compressibility value of $4.5 \times 10^{-5}\,\mathrm{bar}^{-1}$ is applied in the three directions of the simulation box.

To account for the effect of the range of the dispersive interactions on the three-phase coexistence temperature of the hydrates studied at a given pressure, we use different cut-off distances for the dispersive and coulombic interactions. Particularly, we consider four different cut-off values: 0.9, 1.1, 1.3, and 1.6 nm. In terms of reduced units with respect to the molecular size of the oxygen atom of water molecules (see Table I), the cut-off values range from 2.8 to 5, approximately. Besides, two additional sets of simulations have been performed using two different long-range corrections (LRCs) for the dispersive interactions. The first one is the so-called homogeneous LRCs for the dispersive energy and pressure (LRCs-H),[52,53] assuming explicitly that the system is homogeneous. Strictly this is not true because the system exhibits

three phases in equilibrium. However, this methodology has been applied previously in water systems that exhibit one or more phases obtaining good results.[47,63–66] The reason is that the uncertainties incorporated by the LRC, with the assumption that the system is homogeneous, are smaller than the error introduced when simulations are performed using a small cut-off distance.

The second set of LRCs used in this work is the particle mesh Ewald (PME)[58,59] method for dispersive interactions. The PME method has the advantage that the inhomogeneity of the system is explicitly taken into account. Strictly speaking, this is the appropriate set of LRCs that has to be used in systems that exhibit more than one phase in coexistence. However, there exists a limitation for this methodology when using the GROMACS package: it can be only used when unlike dispersive interactions follows the standard geometric Lorentz-Berthelot combining rules. Unfortunately, as it is shown below, this set of LRCs can be only applied in the study of the CH_4 hydrate.

Finally, it is important to note, that for the case of the coulombic interactions, LRCs have been applied in all cases. It means that the coulombic potential is truncated with the same cut-off distance as the dispersive interactions, and then, the particle mesh Ewald (PME) method[58] is applied to take into account the dismissed coulombic interactions. Hence, the effect of using different cut-off distances for the coulombic interactions is negligible because long-range corrections have been applied in all the simulations. The PME range corrections, for all the interactions, have been used with GROMACS default values (a mesh width of 0.1 nm and a relative tolerance of 10^{-5}).

B. Force Fields

Water molecules are modeled using the well-known TIP4P/Ice model.[67] This model has been widely used for the study of the solid phases of water.[44,47,48,63,68] CO_2 molecules are described using the TraPPE force field,[69] and CH_4 molecules are modeled as single Lennard-Jones (LJ) spheres with molecular parameters taken from the work of Guillot and Guissani.[70,71] These models have been previously used by some of us for determining the three-phase coexistence lines of CH_4 and CO_2 hydrates.[44,47,48,54,55,63] Non-bonded interactions between different chemical groups are calculated through the sum of the LJ and the Coulomb intermolecular potentials:

$$U(r_{ij}) = 4\varepsilon_{ij}\left[\left(\frac{\sigma_{ij}}{r_{ij}}\right)^{12} - \left(\frac{\sigma_{ij}}{r_{ij}}\right)^{6}\right] + \frac{q_i q_j}{4\pi\varepsilon_0 r_{ij}} \qquad (1)$$

where r_{ij} is the distance between the chemical groups i and j, σ_{ij} and ε_{ij} are the diameter and well depth associated with the LJ potential, q_i and q_j are the partial charges placed on chemical groups i and j, and ε_0 is the permittivity of vacuum. The molecular parameters associated with each chemical group of water, carbon dioxide, and methane molecules are summarized in Table I. The non-bonded interaction parameters between unlike groups are calculated through the standard Lorentz-Berthelot combining rules except for the water–CO_2(2) interactions. In this case, the crossed interaction energy parameter is calculated as $\varepsilon_{12} = \xi(\varepsilon_{11}\varepsilon_{22})^{1/2}$, with $\xi = 1.13$. This modification of the Berthelot combining rule is necessary in order to accurately predict the three-phase coexistence line of the CO_2 hydrate.[44]

TABLE I. Non-bonded interaction parameters of water,[67] carbon dioxide,[69] and metane.[70,71]

Atom	σ(Å)	ε/k_B(K)	q(e)
Water molecule			
O	3.1668	106.1	-
H	-	-	0.5897
M	-	-	1.1794
Carbon dioxide molecule			
C	2.80	27.0	0.700
O	3.05	79.0	-0.350
Methane molecule			
CH_4	3.73	147.5	-

III. METHODOLOGY

In this work, we determine the three-phase equilibrium coexistence temperature T_3, at several pressures, through the direct coexistence simulation technique. This methodology has been widely applied in the literature for determining the stability conditions of hydrates.[44,48–50] The technique is based on the simulation of the three phases, i.e., the hydrate, aqueous solution, and guest-rich fluid phases (liquid CO_2 and gas CH_4 in our particular case), that coexist in the same simulation box and separated by two planar interfaces. According to the phase rule for non-reacting systems, a binary mixture that exhibits three phases in equilibrium has only one thermodynamic degree of freedom. Since the system is inhomogeneous, we fixed the component of the pressure tensor perpendicular to the planar interfaces. Since we also fixed the temperature of the system, there are three possible scenarios depending on the temperature considered.

If the temperature is above the T_3, the hydrate will melt and only two phases remain stable in the simulation box: the aqueous solution and the CO_2- or the CH_4-rich fluid phase. Contrary, if the temperature is below the T_3, the hydrate will grow until one of the fluid phases disappears (the aqueous solution or the guest-rich fluid phase). Which fluid phase is the remaining depends on the amount of each component used in the simulation box. Finally, there is a third scenario when the temperature of the system matches the T_3. When the system is simulated at the three-phase equilibrium conditions, the hydrate will grow/melt with a 50% probability. It means that if more than one simulation is performed at these conditions, the hydrate will grow/melt in half of them.

Although this procedure has been used in previous works for the determination of the three-phase coexistence line of the CH_4 and CO_2 hydrates, the effect of the range of the dis-

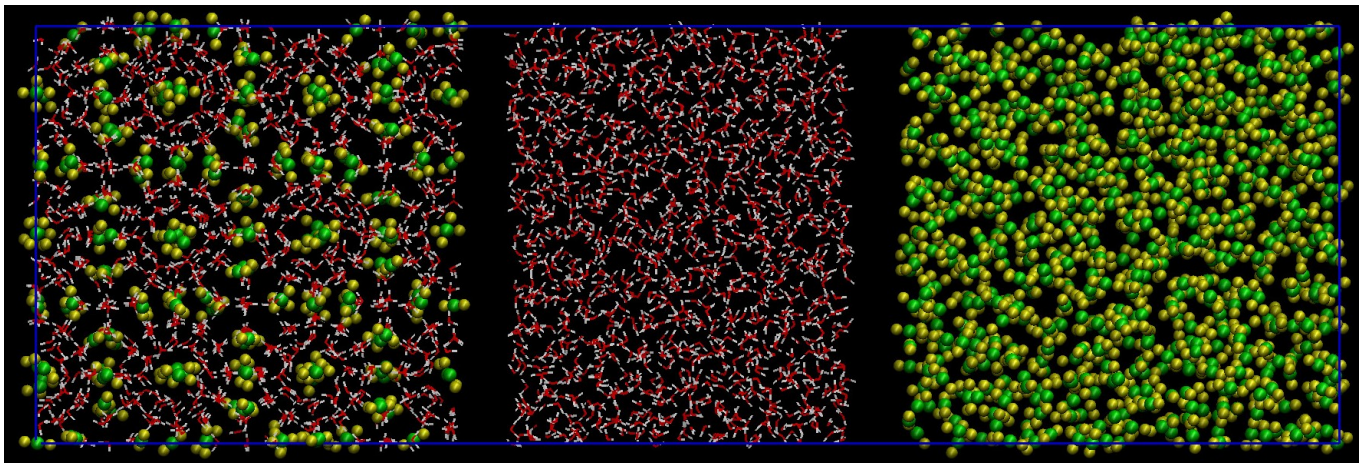

FIG. 1. Representation of the initial simulation box used in this work for the case of the CO_2 hydrate. Red and white spheres represent the oxygen and hydrogen atoms of the water molecules, and green and yellow spheres carbon and oxygen atoms of the CO_2 molecule, respectively. From left to right, the simulation box is conformed by a hydrate phase, a water phase, and a CO_2 phase. For the case of the CH_4 hydrate, the initial simulation box is identical but the CO_2 is replaced by CH_4.

persive interactions on the T_3 has not been properly analyzed. Usually, the size of the hydrate used in the initial simulation boxes in previous works has been $2 \times 2 \times 2$,[44,48–50] which means that the hydrate unit cell has been replicated 2 times in each space direction (368 and 64 molecules of water and guest respectively).

In this work, we use an initial simulation box in which a hydrate phase fully occupied is in contact with a pure water phase and a phase formed from CO_2 or CH_4 molecules depending on the hydrate considered. The hydrate phase is created by replicating 3 times the unit cell in each space direction. The final $3 \times 3 \times 3$ hydrate phase is formed by 1242 and 216 water and guest molecules, respectively. The initial water phase is formed by 1242 water molecules, and the guest phase by 400 molecules (see Table II). Note that the use of this initial simulation box pursues two objectives: (1) to avoid finite-size effects; and (2) to allow the use of cut-off distances up to 1.6 nm. A sketch of the initial simulation box used in this work is presented in Fig. 1 It is important to notice that the election of the final system size is far from being arbitrary. According to the two first papers of the series,[54,55] a non-stoichiometric number of water and guest molecules in the initial aqueous solution and guest-rich phases in combination with a $3 \times 3 \times 3$ hydrate phase allow us to determine accurately the T_3 value without finite-size effects (we refer the lector to papers I[54] and II[55] for further details). Also, it is interesting to mention that the empty space between phases shown in Fig. 1 is rapidly occupied by the water solution and guest-rich phases in the first steps of the simulation. The initial gap between phases prevents the overlapping of the molecules of each phase when they are placed together in the same simulation box.

Hydrate phase			Water solution	Guest-rich phase
Unit Cell	Water	CO_2/CH_4	Water	CO_2/CH_4
3x3x3	1242	216	1242	400

TABLE II. Initial number of molecules in the hydrate phase, water solution phase, and guest-rich phase. The same configuration for methane and carbon dioxide has been used in all the simulations carried out in this work.

IV. RESULTS

We have performed simulations at three different pressures in the case of the CO_2 hydrate: 100, 400, and 1000 bar. However, we only perform simulations at 400 bar in the case of the CH_4 hydrate. The reason is that simulation times needed to observe growth or melt in the case of the CH_4 hydrate are much longer than in the case of the CO_2 hydrate due to the low solubility exhibited by CH_4 in water. In both cases, the T_3 has been obtained using 4 different cut-off distances for the dispersive interactions: 0.9, 1.1, 1.3, and 1.6 nm. The same cut-off distance is used for the coulombic part of the intermolecular potential. As it has been explained in Section II, we apply PME corrections for the coulombic interactions. We also analyze the effect of using LRCs on the dissociation temperature of each hydrate. To this end, we have carried out additional simulations using two different schemes to account for the LRCs of the dispersive interactions with a cut-off distance equal to 0.9 nm. Particularly, we use the standard LRC-H corrections for both hydrates, and in the case of the CH_4 hydrate, we also used the LRC-PME corrections.

A. CO_2 Hydrate

We first analyze the effect of cut-off distance on the dissociation temperatures of the CO_2 hydrate. At each pressure, we

perform simulations at five temperatures in order to analyze the behavior of the system. Particularly, the temperatures considered are separated by 2 K. Due to the inherent stochasticity of the direct coexistence technique, at temperatures close to the T_3 we run two independent simulations for each cut-off value. This is done to increase the accuracy of the determination of the T_3.

At 100 bar, simulations are performed at temperatures from 281 to 289 K. As can be seen in Figs. 2 and 3, the T_3 value increases as the cut-off distance is increased. In particular, we obtain 284(1), 286(1), 287(1), and 288(1) for cut-off distances of 0.9, 1.1, 1.3, and 1.6 nm, respectively. The main result is that an increase in the range of the dispersive interactions provokes an increase in the stability of the solid phase, allowing the hydrate to be stable at higher temperatures. Particularly, the T_3 value at 100 bar increases from 284(1) K, when a cut-off distance of 0.9 nm is used, to 288(1) K when the cut-off distance is 1.6 nm, as it is clearly shown in Fig. 3.

It is important to compare the results obtained in this work with the data presented by Míguez *et al.*[44] several years ago, as well as with experimental data. The T_3 value obtained with a cut-off distance equal to 0.9 nm, 284(1) K, is in excellent agreement with the result obtained by Míguez *et al.*, 284(2) K, using a cut-off value of 1.0 nm. The result is also in good agreement with experimental data taken from the literature (283.6 K).[1] Note that when the cut-off value is increased, the simulation results slightly overestimate the experimental value. Why does agreement between experimental data and simulation results become worse as the cut-off distance increases? The reason is related to the election of the modified Berthelot combining rule. The value of the water-CO_2 unlike the dispersion interaction used in this work, $\xi = 1.13$, was initially proposed by Míguez and collaborators several years ago.[44] In that work, the cut-off distance for the dispersive interactions used was $r_c = 1.0$ nm. In addition to that, the system size used was much smaller than that used in this work. Note that, not only the cut-off distance affects the location of the dissociation temperature at a given pressure but also the size of the simulated system. We recommend the reader the papers I and II of this series to understand the finite-size effects on phase equilibria of hydrates.[54,55]

The effect of using LRC-H corrections on the location of the T_3 has been also analyzed in this work. As explained in Sec. II A, the use of LRC-H is not strictly correct when several phases coexist in the same simulation box, i.e., when the system is inhomogeneous. However, this methodology has been applied before in the literature to describe multi-phase systems improving the accuracy of the results.[47,63–66] This is because the difference between the simulation predictions using the full and a truncated intermolecular potential using a small cut-off value is bigger than using the LRC-H corrections assuming a homogeneous system. As can be seen in Fig. 3, the use of the LRC-H with a cut-off value of 0.9 nm increase significantly the prediction of the T_3, from 284(1) K ($r_c = 0.9$ nm and no corrections), to 287(1) K ($r_c = 0.9$ nm and LRC-H corrections). Note that the value of T_3 obtained is the same, within the error bars as those obtained using $r_c = 1.3$ and 1.6 nm.

Before finishing the analysis of the results obtained at 100 bar, it is important at this point to remark that an increase in the cut-off value implies an increment of the computational effort necessary to perform the simulations. Indeed, LRCs are routinely used to reduce the computational effort without lost accuracy. Particularly, simulations performed using $r_c = 0.9$ nm with and without LRC-H require the same CPU time. However, simulations performed using a cut-off value of 0.9 nm are, on average, three times faster than simulations with a cut-off value of 1.6 nm.

Following the same procedure used to determine the dissociation temperature of the CO_2 hydrate at 100 bar, we perform simulations at temperatures from 284 to 292 K to estimate the T_3 at 400 bar using different cut-off distances. Particularly, we obtain 287(1), 289(1), 290(1), and 290(1) K for cut-off distances equal to 0.9, 1.1, 1.3, and 1.6 nm, respectively. As can be seen, there is no influence of the cut-off value on the results when using $r_c = 1.3$ and 1.6 nm. It is also interesting to note that the difference between the results obtained using 0.9 and 1.6 nm cut-off distances is smaller now (3 instead of 4 K obtained at 100 bar). Although the T_3 values are within the uncertainties bars, it seems that the cut-off value used to deal with the dispersive interactions has less effect on T_3 as the pressure increases. It is also important to compare the results obtained in this work with the predictions previously presented in the literature, as well as with experimental data taken from the literature. The T_3 value obtained with a cut-off distance of 0.9 nm, 287(1) K, is in excellent agreement with the result obtained by Míguez *et al.*,[44] 287(2) K. The T_3 of the CO_2 hydrate at 400 bar has been also obtained very recently by some of us using the so-called solubility method.[56] In this work, the T_3 values obtained were 290(2) and 292(2) K for cut-off distances equal to 1.0 and 1.9 nm, respectively. Although all the results are in good agreement, within the uncertainties bars, care must be taken when comparing with data from the literature obtained using different system sizes. As we have already discussed in our previous papers I and II, the finite-size effects can affect the value of the dissociation temperature of hydrates obtained from computer simulation.[54,55]

It is also interesting to compare the values of the T_3 obtained using different cut-off distances with experimental data taken from the literature. At 400 bar, $T_3 = 286.2$ K.[1] As it happens at 100 bar, when the cut-off value is increased the simulation results slightly overestimate the experimental data. As we have mentioned previously, this is due because the Berthelot rule was adjusted using a cut-off distance $r_c = 1.0$ nm[44] and we now are using higher cut-off distances with the same ξ parameter value.

We have also analyzed the impact of using LRC-H corrections on the determination of the dissociation temperature of the hydrate at 400 bar. As it is shown in Fig. 3, the dissociation temperature obtained using a cut-off distance of 0.9 nm and LRC-H is 288(1) K. This value is slightly outside the error bar when it is compared with the data obtained using $r_c = 1.6$ nm.

To finish this Section, we finally consider the effect of the cut-off distance on the dissociation temperature of the hydrate at 1000 bar. To this end, we have performed simula-

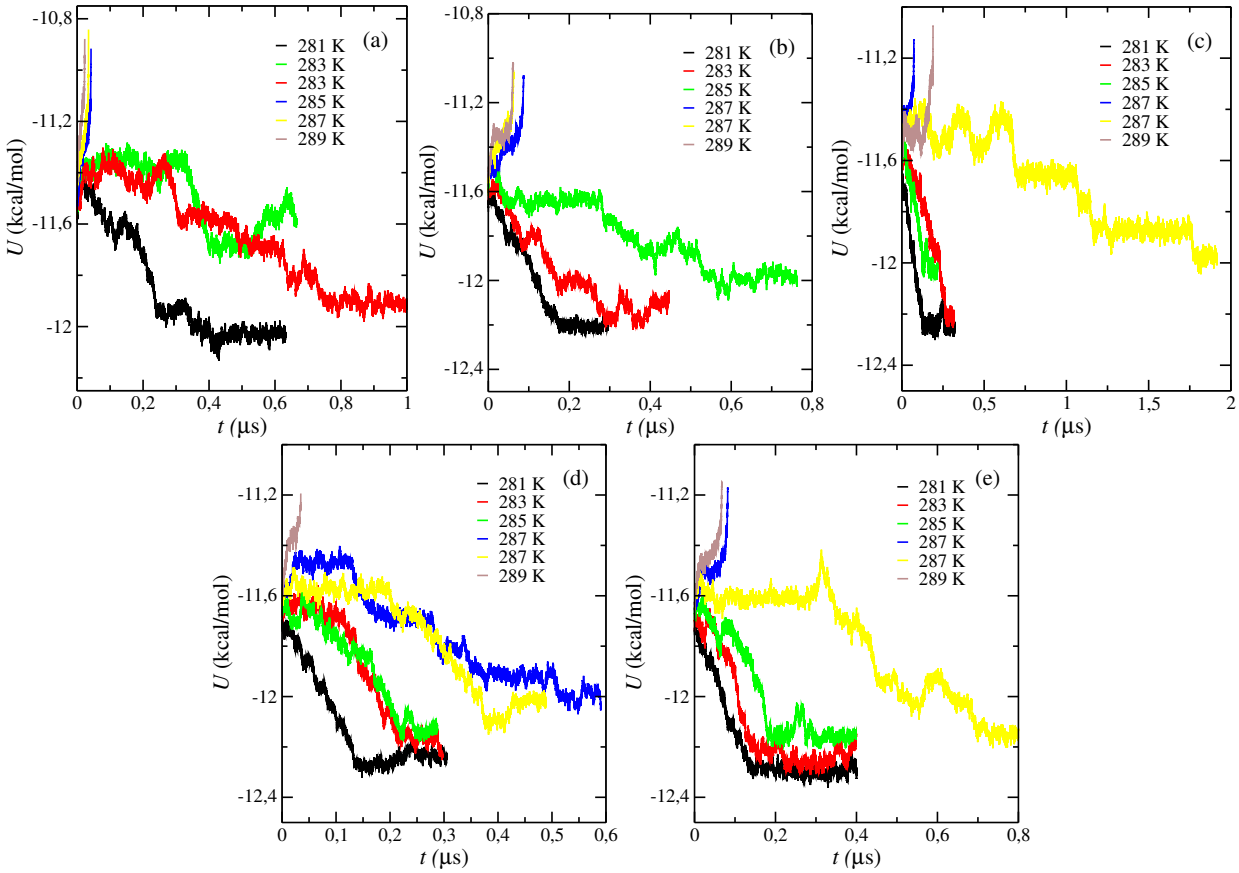

FIG. 2. Potential energy, as a function of time, at 1000, bar and different temperatures for different cut-off values: (a) 0.9 nm, (b) 1.1 nm, (c) 1.3 nm, (d) 1.6 nm, and (e) 0.9 nm + LRC-H. Notice that large simulation times are necessary when the temperature is close to the T_3 value.

tions at temperatures from 286 to 294 K. At this pressure, the effect of the cut-off distance seems to be negligible for values $r_c \geq 1.1$ nm. Particularly, $T_3 = 291(1)$ K when using $r_c = 0.9$ nm and $T_3 = 293(1)$ K when using all of the rest cutoff distances, $r_c = 1.1$, 1.3, and 1.6 nm. The dissociation temperature of the hydrate is also equal to 293(1) K when the cut-off distance is equal to 0.9 nm using LRC-H. All the results obtained at 1000 bar, are summarized is Fig. 3. It is also interesting to compare the predictions obtained in this work with the data calculated by some of us in a previous work,[44] as well as with experimental data taken from the literature.[1] The dissociation temperature of the CO_2 hydrate at 1000 bar obtained by Míguez *et al.*[44] is $T_3 = 289(2)$ K and the experimental temperature at the same condition $T_{exp} = 289$ K. As can be seen, the results obtained in this work slightly overestimate the previous results, as well as the experimental value. This disagreement between the data obtained in this work and previous results of Míguez *et al.*[44] and experimental data[1] are directly related to the effect of dispersive interactions of the intermolecular potential used in the simulations. The T_3 values obtained in this work for the CO_2 hydrate at each pressure and each cut-off have been summarized in Table III.

It is interesting to recall here the main conclusion of the effect of dispersive interactions on the dissociation temperature of the CO_2 hydrate at different pressures. As can be seen

CO_2 Hydrate T_3 (K)							
P (bar)	Expt.	0.9 nm	1.1 nm	1.3 nm	1.6 nm	0.9 nm +LRC-H	0.9 nm +LRC-IH
100	283.6	284(2)	286(2)	287(2)	288(2)	287(2)	-
400	286.2	287(2)	289(2)	290(2)	290(2)	288(2)	-
1000	289.7	291(2)	293(2)	293(2)	293(2)	293(2)	-
CH_4 Hydrate T_3 (K)							
400	297	291(1)	291(1)	293(1)	295(1)	294(1)	294(1)

TABLE III. Dissociation temperature of the CO_2 and CH_4 hydrates as a function of the cut-off value at each pressure studied in this work.

in Fig. 3, the effect of the cut-off distance on the T_3 value depends on pressure: its effect is very important at the lowest pressure considered and it decreases as the pressure is increased. Particularly, when pressure is high enough, there is no effect of the cut-off distance on the stability conditions of the hydrate. In terms of efficiency, this should be taken into account because the use of a small cut-off distance provides the same result as that using a large cut-off value with a decrease in the computational cost. If simulations are performed using a cut-off distance of 1.6 nm, then simulations using cut-off distances of 1.3, 1.1, and 0.9 nm (with or without LRC-H) are 1.5, 2.1, and 3 faster, respectively. It is clear from this discussion that, not only the system size affect the dissociation

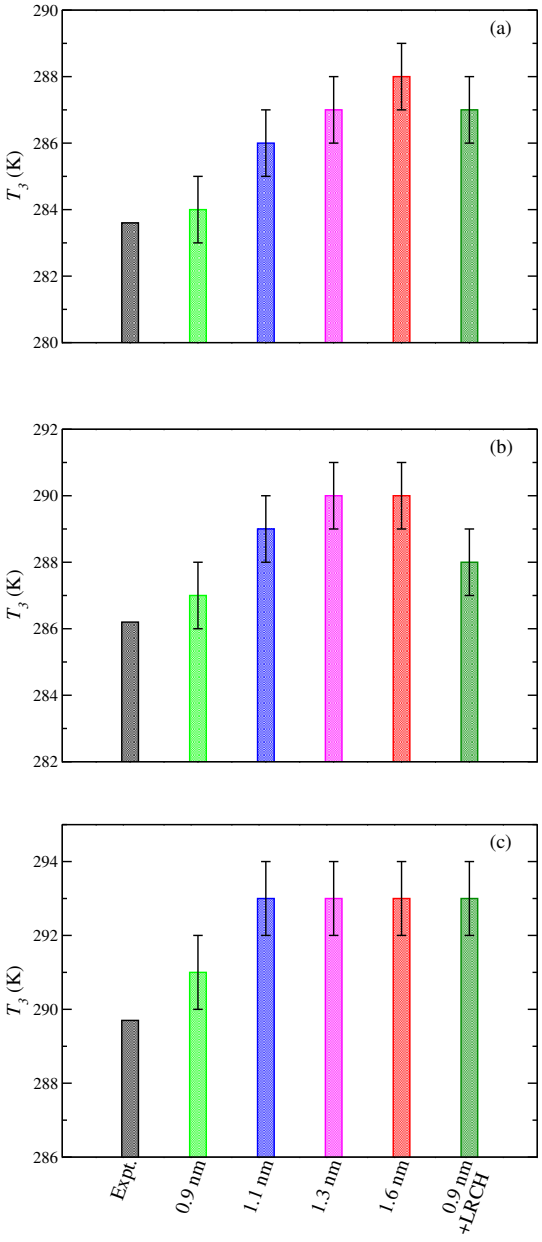

FIG. 3. Dissociation temperature of the CO_2 hydrate, as a function of the cut-off distance, at (a) 100 bar, (b) 400 bar, and (c) 1000 bar. Results obtained in this work are presented as black bars and uncertainties as red lines.

temperature of a hydrate, as it is shown in our previous papers I and II,[54,55] but also the election of the cut-off distance strongly affects the dissociation temperature of hydrates.

Finally, an additional clarification is needed on the relation between the cut-off distance and the unlike intermolecular interactions for the CO_2 hydrate. Contrary to what happens with the CH_4 hydrate, in the case of the CO_2 hydrate it is necessary to fit the unlike water–carbon dioxide dispersive interaction to obtain a quantitative description of the dissociation temperature of this hydrate as it was shown several years ago by Míguez *et al.*[44] and Costandy *et al.*[50] The election of the optimal value of ξ in both studies was done using a relatively small cut-off distance and system size. Particularly, both studies used $r_c = 1.0$ and 0.9 nm, respectively, and a hydrate seed obtained replicating the unit cell 2 times along each space direction ($2 \times 2 \times 2$). Using these parameters, it was possible to provide an excellent agreement between simulation and experiments, particularly in the case of the study by Míguez *et al.*[44] In this work, however, we use larger cut-off distances and a larger hydrate seed ($3 \times 3 \times 3$). As a consequence of this, agreement between simulations and experimental data taken from the literature becomes worse as the cut-off distance increases. This is a direct consequence of fitting ξ using a particular set of r_c value and system size. If a better agreement between simulation and experiments is needed, a new modification of the Berthelot rule should be developed using larger cut-off distances and system sizes in order to match the experimental data.[1] Unfortunately, this is out of the scope of this work.

B. CH_4 Hydrate

We now examine the effect of the cut-off distance on the T_3 of the CH_4 hydrate. For this purpose, we have used the same system size employed for the CO_2 hydrate (see Table II). Note that methane hydrate usually requires larger simulation times (typically, simulation times are of the order of μs) than those used for the CO_2 hydrate to observe either growth or melt. This is due to the high solubility of CO_2 in water, about ten more times, compared with that of CH_4 in water. In Figure 4, we show the potential energy, as a function of time, of the studied system at 400 bar and different temperatures using several cut-off distances. Similarly, we have used four distinct values, ranging from 0.9 to 1.6 nm, as in the case of the CO_2 hydrate. Additionally, we have implemented two different LRCs with $r_c = 0.9$ nm. On one hand, we have incorporated the same LRC-H corrections for dispersive energy and pressure than in the study of the CO_2 hydrate. It is important to note that these corrections can be only applied if the system is homogeneous. This is not the case of systems under study since we are simulating inhomogeneous systems in which gas, liquid, and solid phases coexist via planar interfaces. On the other hand, we have applied LRCs using the PME method for dispersive interactions, which is valid for inhomogeneous systems (LRC-I).

The analysis of the potential energies, as functions of time, yields several notable findings. Firstly, it is evident that the time required for this hydrate to melt or grow is significantly longer compared to that of the CO_2 hydrate. In fact, we have conducted multiple simulations in which the CH_4 hydrate needs more than 2 μ to grow. Note that in the case of the CO_2 hydrate, the longest time observed for growing is only 1 μ. This behavior aligns with both experimental[72–78] and *in silico*[79,80] observations, which consistently show that the CH_4 hydrate exhibits larger growth rates compared to those of the CO_2 hydrate.

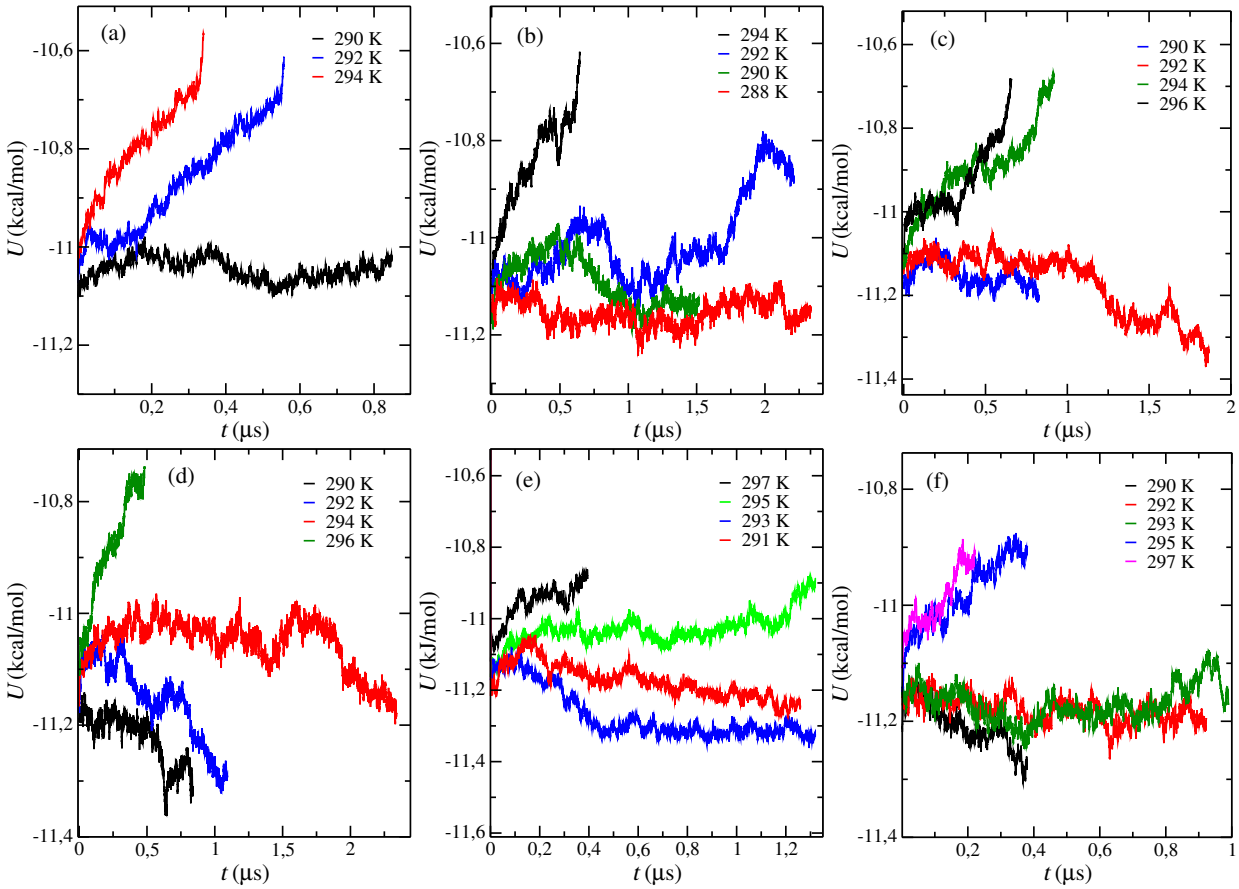

FIG. 4. Potential energy, as a function of time, at 400 bar and different temperatures for different cut-off values for the methane hydrate-water-gas methane system: (a) 0.9 nm, (b) 1.1 nm, (c) 1.3 nm, (d) 1.6 nm, (e) 0.9 nm + LRC-H, and (f) 0.9 nm + LRC-I.

Secondly, the dissociation temperature T_3 varies with each cut-off distance used in simulations. Fig. 5 displays the T_3 obtained using different cut-off distances in a bar chart. It is evident that T_3 increases as the cut-off value is increased. This trend mirrors that observed in the case of the CO_2 hydrate, indicating a common behavior in both systems with respect to cut-off values. Notice that at the same pressure (400 bar) for the CO_2 the T_3 increases in 2 K when going from 0.9 nm to 1.1 nm in the cut-off, whereas in the case of methane we observe an increment of 1 K. It is neccesary to apply the LRC in this system to observe the increment of 2 K.

As in Section IV A, we have also performed simulations using a cut-off distance of 0.9 nm along with LRC to both energy and pressure. As can be seen, we also observe a notable increase in the T_3 value when compared to that obtained using $r_c = 0.9$ nm without any LRC. It is interesting to compare the predictions obtained using this value of cut-off in combination with homogeneous (LRCH) and inhomogeneous (LRCI) corrections. As can be seen, the T_3 obtained in both cases is identical and also very close to the value obtained with $r_c = 1.6$ nm. In fact, when considering the associated error bars, the dissociation temperatures are practically the same.

To finish this section, it is worthy to mention the efficiency in terms of computational cost. According to Fig. 5, simulations using a cut-off distance $r_c = 0.9$ nm, in combination with LRCs, and using a cut-off distance $r_c = 1.6$ nm predict virtually identical dissociation temperatures within the error bars. It is important to take into account that simulations needed to distinguish if the hydrate grows or melts take 2μs of simulated time in most cases. According to this, we recommend conducting simulations using a cut-off distance equal to 0.9 nm and the inclusion of LRCs for the case of the CH_4 hydrate. This approach not only conserves computational resources but also yields results that are consistent with the higher computational cost option, making it a more efficient and practical choice. The T_3 values obtained in this work for the CH_4 hydrate at 400 bar and each cut-off have been summarized in Table III.

V. CONCLUSIONS

In this work, we have employed the direct coexistence simulation technique to study the three-phase equilibria of CO_2 and CH_4 hydrates. The dissociation temperature, T_3, of both hydrates, has been previously studied by some of us.[44,48] Nevertheless, in this case, we have used a larger system to avoid finite-size effects[68]. By employing this system size for both

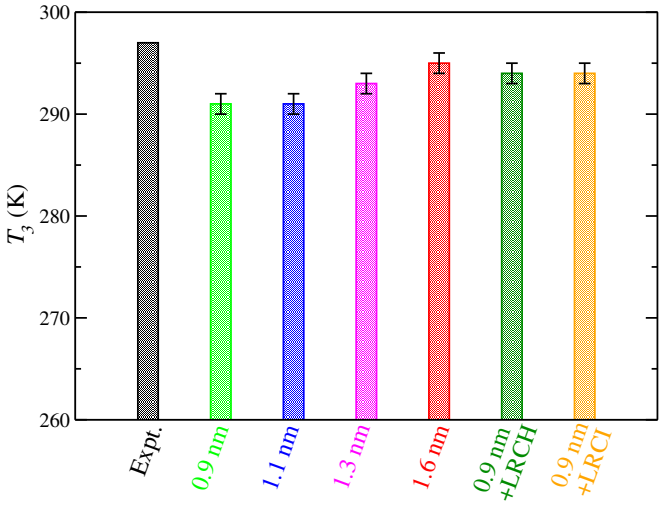

FIG. 5. Dissociation temperature of the CH_4 hydrate, at 400 bar, as a function of the cut-off distance. Results obtained in this work are presented as colored bars and uncertainties as black lines.

hydrates, namely, CO_2 hydrate–aqueous solution–liquid CO_2 and CH_4 hydrate–aqueous solution–gas CH_4, we have performed simulations using different cut-off distances to elucidate its role in the determination of the T_3 of both hydrates.

Our initial investigation focuses on examining the impact of cut-off distance on the dissociation temperature of the CO_2 hydrate at various pressures. We observe that the influence of the cut-off distance on the T_3 is more significant at lower pressures. Specifically, at 100 and 400 bar, increasing the cut-off value produces an increase in T_3. However, at 1000 bar, the effect of the cut-off on the dissociation temperature becomes negligible for $r_c \geq 1.1$ nm. This suggests that the effect of the cut-off value on T_3 is pressure-dependent, with a more pronounced effect at lower pressures.

Once we study the effect of the cut-off on the dissociation temperature of the CO_2 hydrate at different pressures, we consider a hydrate with a different guest. For its interesting applications, we select the CH_4 hydrate for this work. We concentrate only on one pressure, 400 bar, since simulation times required at lower temperatures are computationally expensive. In this case, we find the same effect observed for the CO_2 hydrate, i.e., an increase of the cut-off values yields a rise of the T_3 of the CH_4 hydrate.

Based on the preceding findings, a pressing question arises: What cut-off value should be employed to accurately predict the T_3 for both hydrates? Unfortunately, there is not a definitive answer to this query. Our observations reveal varying scenarios contingent upon pressure conditions. For instance, in the case of the CO_2 hydrate at 100 bar, the most precise predictions are achieved with a 1.6 nm cut-off value. However, at 400 bar, a smaller 1.3 nm cut-off suffices. Finally, at 1000 bar, the use of $r_c = 0.9$ nm and LRCs proves adequate for providing a reliable T_3 estimation. Conversely, using a different guest molecule in the hydrate, CH_4, the situation changes. In the case of methane at 400 bar, a 0.9 nm cut-off distance and LRCs yields reasonably T_3 estimations. There exists no universally applicable answer to the previously mentioned question. The impact of the cut-off value is contingent on both the guest molecule and the prevailing pressure conditions. In essence, each system is different and necessitates a thorough investigation to determine the most suitable cut-off distance for the precise estimation of T_3 However, as we previsouly mentioned, we recommend simulating using the cut-off of 0.9 nm and applying LRCs. In this way, we are able to simulate the system with affordable computational resources and to obtain accurate results for the T_3.

In summary, this work provides valuable insights into the intricate process of computing the dissociation line of hydrates. It suggests a specific cut-off value that can yield accurate estimations of T_3 for the examined force fields without necessitating excessively time-consuming simulations. This finding contributes to the optimization of computational resources while maintaining the reliability of the results in the study of hydrate systems.

ACKNOWLEDGMENTS

This work was funded by Ministerio de Ciencia e Innovación (Grant No.PID2019-105898GA-C22, PID2021-125081NB-I00 and PID2022-136919NB-C32), Junta de Andalucía (P20-00363), and Universidad de Huelva (P.O. FEDER UHU-1255522 and FEDER-UHU-202034), all four cofinanced by EU FEDER funds. This work was also funded by Project No. ETSII-UPM20-PU01 from "Ayudas Primeros Proyectos de la ETSII-UPM". M.M.C. acknowledges CAM and UPM for financial support of this work through the CavItieS project No. APOYO-JOVENES-01HQ1S-129-B5E4MM from "Accion financiada por la Comunidad de Madrid en el marco del Convenio Plurianual con la Universidad Politecnica de Madrid en la linea de actuacion estimulo a la investigacion de jovenes doctores" and CAM under the Multiannual Agreement with UPM in the line Excellence Programme for University Professors, in the context of the V PRICIT (Regional Programme of Research and Technological Innovation). S.B. acknowledges Ayuntamiento de Madrid for a Residencia de Estudiantes grant. The authors also gratefully acknowledge the Universidad Politecnica de Madrid (www.upm.es) for providing computing resources on Magerit Supercomputer. We also acknowledge additional computational resources from Centro de Supercomputación de Galicia (CESGA, Santiago de Compostela, Spain), at which some of the simulations were run.

AUTHORS DECLARATIONS

CONFLICTS OF INTEREST

The authors have no conflicts to disclose.

DATA AVAILABILITY

The data that support the findings of this study are available within the article.

REFERENCES

[1] E. D. Sloan and C. Koh, *Clathrate Hydrates of Natural Gases*, 3rd ed. (CRC Press, New York, 2008).

[2] B. C. Barnes and A. K. Sum, "Advances in molecular simulations of clathrate hydrates," Current Opinion in Chemical Engineering **2**, 184–190 (2013).

[3] K. A. Kvenvolden, "Methane hydrate – a major reservoir of carbon in the shallow geosphere?" Chem. Geol. **71**, 41–51 (1988).

[4] C. A. Koh, A. K. Sum, and E. D. Sloan, "State of the art: Natural gas hydrates as a natural resource," J. Nat. Gas Sci. Eng. **8**, 132–138 (2012).

[5] "World Energy Outlook 2022," Tech. Rep. (International Energy Agency, Paris, 2022).

[6] M. Yand, Y. Song, L. Jiang, Y. Zhao, X. Ruan, Y. Zhang, and S. Wang, "Hydrate-based technology for CO_2 capture from fossil fuel power plants," Appl. Energy **116**, 26–40 (2014).

[7] M. Ricaurte, C. Dicharry, X. Renaud, and J.-P. Torré, "Combination of surfactants and organic compounds for boosting CO_2 separation from natural gas by clathrate hydrate formation," Fuel **122**, 206–217 (2014).

[8] B. Kvamme, G. A, T. Buanes, T. Kuznetsova, and G. Ersland, "Storage of CO_2 in natural gas hydrate reservoirs and the effect of hydrate as an extra sealing in cold aquifers," Int. J. Greenhouse Gas Control **1**, 236–246 (2007).

[9] W. L. Mao, H. K. Mao, A. F. Goncharov, V. V. Struzhkin, Q. Guo, J. Hu, J. Shu, R. J. Hemley, M. Somayazulu, and Y. Zhao, "Hydrogen clusters in clathrate hydrate," Science **297**, 2247–2249 (2002).

[10] W. L. Mao and H. K. Mao, "Hydrogen storage in molecular compounds," Proc. Natl. Acad. Sci. **101**, 708–710 (2004).

[11] H. Lee, J.-w. Lee, D. Y. Kim, J. Park, Y.-T. Seo, H. Zeng, I. L. Moudrakovski, C. I. Ratcliffe, and J. A. Ripmeester, "Tuning clathrate hydrates for hydrogen storage," Nature **434**, 743–746 (2005).

[12] H. P. Veluswamy, R. Kumar, and P. Linga, "Hydrogen storage in clathrate hydrates: Current state of the art and future directions," Applied Energy **122**, 112–132 (2014).

[13] S. Y. Willow and S. S. Xantheas, "Enhancement of hydrogen storage capacity in hydrate lattices," Chemical Physics Letters **525**, 13–18 (2012).

[14] L. J. Florusse, C. J. Peters, J. Schoonman, K. C. Hester, C. A. Koh, S. F. Dec, K. N. Marsh, and E. D. Sloan, "Stable low-pressure hydrogen clusters stored in a binary clathrate hydrate," Science **306**, 469–471 (2004).

[15] T. A. Strobel, C. A. Koh, and E. D. Sloan, "Hydrogen storage properties of clathrate hydrate materials," Fluid Phase Equilibria **261**, 382–389 (2007).

[16] T. Sugahara, J. C. Haag, P. S. Prasad, A. A. Warntjes, E. D. Sloan, A. K. Sum, and C. A. Koh, "Increasing hydrogen storage capacity using tetrahydrofuran," Journal of the American Chemical Society **131**, 14616–14617 (2009).

[17] A. Davoodabadi, A. Mahmoudi, and H. Ghasemi, "The potential of hydrogen hydrate as a future hydrogen storage medium," Iscience **24** (2021).

[18] Y. H. Hu and E. Ruckenstein, "Clathrate hydrogen hydrate—a promising material for hydrogen storage," Angewandte Chemie International Edition **45**, 2011–2013 (2006).

[19] S.-P. Kang, H. Lee, C.-S. Lee, and W.-M. Sung, "Hydrate phase equilibria of the guest mixtures containing co_2, n_2 and tetrahydrofuran," Fluid Phase Equil. **185**, 101–109 (2001).

[20] A. Delahaye, L. Fournaison, S. Marinhas, and I. Chatti, "Effect of thf on equilibrium pressure and dissociation enthalpy of co_2 hydrates applied to secondary refrigeration," Ind. Eng. Chem. Res. **45**, 391–397 (2006).

[21] R. Anderson, A. Chapoy, and B. Tohidi, "Phase relations and binary clathrate hydrate formation in the system h_2-thf-h_2o," Langmuir **23**, 3440–3444 (2007).

[22] Y.-J. Lee, T. Kawamura, Y. Yamamoto, and J.-H. Yoon, "Phase equilibrium studies of tetrahydrofuran (thf) + ch_4, thf + co_2, ch_4 + co_2, and thf + co_2 + ch_4 hydrates," J. Chem. Eng. Data **57**, 3543–3548 (2012).

[23] A. Striolo, A. Phan, and M. R. Walsh, "Molecular properties of interfaces relevant for clathrate hydrate agglomeration," Current Opinion in Chemical Engineering **25**, 57–66 (2019).

[24] T. Bui, A. Phan, D. Monteiro, Q. Lan, M. Ceglio, E. Acosta, P. Krishnamurthy, and A. Striolo, "Evidence of structure-performance relation for surfactants used as antiagglomerants for hydrate management," Langmuir **33**, 2263–2274 (2017).

[25] T. Bui, F. Sicard, D. Monteiro, Q. Lan, M. Ceglio, C. Burress, and A. Striolo, "Antiagglomerants affect gas hydrate growth," The Journal of Physical Chemistry Letters **9**, 3491–3496 (2018).

[26] A. Phan, T. Bui, E. Acosta, P. Krishnamurthy, and A. Striolo, "Molecular mechanisms responsible for hydrate anti-agglomerant performance," Physical Chemistry Chemical Physics **18**, 24859–24871 (2016).

[27] P. M. Naullage, A. A. Bertolazzo, and V. Molinero, "How do surfactants control the agglomeration of clathrate hydrates?" ACS Central Science **5**, 428–439 (2019).

[28] P. M. Naullage and V. Molinero, "Slow propagation of ice binding limits the ice-recrystallization inhibition efficiency of pva and other flexible polymers," Journal of the American Chemical Society **142**, 4356–4366 (2020).

[29] L. C. Jacobson, W. Hujo, and V. Molinero, "Amorphous precursors in the nucleation of clathrate hydrates," Journal of the American Chemical Society **132**, 11806–11811 (2010).

[30] J. Lederhos, J. Long, A. Sum, R. Christiansen, and E. Sloan Jr, "Effective kinetic inhibitors for natural gas hydrates," Chemical Engineering Science **51**, 1221–1229 (1996).

[31] R. Wu, Z. M. Aman, E. F. May, K. A. Kozielski, P. G. Hartley, N. Maeda, and A. K. Sum, "Effect of kinetic hydrate inhibitor polyvinylcaprolactam on cyclopentane hydrate cohesion forces and growth," Energy & fuels **28**, 3632–3637 (2014).

[32] F. Wang, A. K. Sum, and B. Liu, "Recent advances in promoters for gas hydrate formation," Frontiers in Chemistry **9**, 708269 (2021).

[33] J.-H. Sa and A. K. Sum, "Promoting gas hydrate formation with ice-nucleating additives for hydrate-based applications," Applied Energy **251**, 113352 (2019).

[34] J.-P. Torré, M. Ricaurte, C. Dicharry, and D. Broseta, "Co2 enclathration in the presence of water-soluble hydrate promoters: Hydrate phase equilibria and kinetic studies in quiescent conditions," Chemical engineering science **82**, 1–13 (2012).

[35] J. Ripmeester and C. Ratcliffe, "The diverse nature of dodecahedral cages in clathrate hydrates as revealed by ^{129}Xe and ^{13}C Nmr spectroscopy: CO_2 as a small-cage guest," Energy Fuels **12**, 197 (1998).

[36] T. Ikeda, O. Yamamuro, T. Matsuo, K. Mori, S. Torii, T. Kamiyama, F. Izumi, S. Ikeda, and S. Mae, "Neutron diffraction study of carbon dioxide clathrate hydrate," J. Phys. Chem. Solids **60**, 1527 (1999).

[37] K. Udachin, C. Ratcliffe, and J. Ripmeester, "Structure, composition, and thermal expansion of CO_2 hydrate from single crystal X-Ray diffraction measurements," J. Phys. Chem. B **105**, 4200 (2001).

[38] S. Nakano, M. Moritoki, and K. Ohgaki, "High-pressure phase equilibrium and raman microprobe spectroscopic studies on the co2 hydrate system," J. Chem. Eng. Data **43**, 807–810 (1998).

[39] R. Henning, A. Schultz, V. Thieu, and Y. Halpern, "Neutron diffraction studies of CO_2 clathrate hydrate: Formation from deuterated ice," J. Phys. Chem. A **104**, 5066 (2000).

[40] D. H. Smith, K. Seshadri, T. Uchida, and J. W. Wilder, "Thermodynamics of methane, propane, and carbon dioxide hydrates in porous glass," AIChE Journal. **50**, 1589–1598 (2004).

[41] S.-P. Kang, J.-W-Lee, and H.-J. Ryu, "Phase behavior of methane and carbon dioxide hydrates in meso- and macro-sized porous media," Fluid Phase Equil. **274**, 68–72 (2008).

[42] J. C. Platteeuw and J. H. van der Waals, "Thermodynamic properties of gas hydrates," Mol. Phys. **1**, 91–96 (1957).

[43] J. C. Platteeuw and J. H. V. der Waals, "Thermodynamic properties of gas hydrates II: Phase equilibria in the system H_2S-C_3H_3-H_2O at -3°C," Rec. Trav. Chim. Pays Bas **78**, 126–133 (1959).

[44] J. M. Míguez, M. M. Conde, J.-P. Torré, F. J. Blas, M. M. Piñeiro, and C. Vega, "Molecular dynamics simulation of CO_2 hydrates: Prediction of three phase coexistence line," J. Chem. Phys. **142**, 124505–1–124505–12 (2015).

[45] M. Pérez-Rodríguez, A. Vidal-Vidal, J. Míguez, F. J. Blas, J.-P. Torré, and M. M. Piñeiro, "Computational study of the interplay between intermolec-

ular interactions and CO_2 orientations in type I hydrates," Phys. Chem. Chem. Phys. **19**, 3384–3393 (2017).

[46] A. M. Fernàndez-Fernàndez, M. Pérez-Rodríguez, A. Comesana, and M. M. Pineiro, "Three-phase equilibrium curve shift for methane hydrate in oceanic conditions calculated from molecular dynamics simulations," J. Mol. Liq. **274**, 426–433 (2019).

[47] J. Grabowska, S. Blázquez, E. Sanz, I. M. Zerón, J. Algaba, J. M. Míguez, F. J. Blas, and C. Vega, "Solubility of methane in water: some useful results for hydrate nucleation," J. Phys. Chem. B **126**, 8553–8570 (2022).

[48] M. M. Conde and C. Vega, "Determining the three-phase coexistence line in methane hydrates using computer simulations," J. Chem. Phys. **133**, 064507 (2010).

[49] V. K. Michalis, J. Costandy, I. N. Tsimpanogiannis, A. K. Stubos, and I. G. Economou, "Prediction of the phase equilibria of methane hydrates using the direct phase coexistence methodology," J. Chem. Phys. **142**, 044501 (2015).

[50] J. Costandy, V. K. Michalis, I. N. Tsimpanogiannis, A. K. Stubos, and I. G. Economou, "The role of intermolecular interactions in the prediction of the phase equilibria of carbon dioxide hydrates," J. Chem. Phys. **143**, 094506 (2015).

[51] J. Algaba, M. J. Torrejón, and F. J. Blas, "Dissociation line and driving force for nucleation of the nitrogen hydrate from computer simulation," The Journal of Chemical Physics, in press (2023), https://doi.org/10.1063/5.0176120.

[52] D. Frenkel and B. Smit, *Understanding Molecular Simulations* (2nd Ed. Academic, San Diego, 2002).

[53] M. P. Allen and D. J. Tildesley, *Computer Simulation of Liquids* (Claredon, Oxford, 1987).

[54] S. Blazquez, J. Algaba, J. M. Míguez, C. Vega, F. J. Blas, and M. M. Conde, "Three-phase equilibria of hydrates from computer simulation. I. Finite-size effects in the methane hydrate," The Journal of Chemical Physics, accepted (2023).

[55] J. Algaba, S. Blazquez, E. Feria, J. M. Míguez, M. M. Conde, and F. J. Blas, "Three-phase equilibria of hydrates from computer simulation. II. Finite-size effects in the carbon dioxide hydrate," The Journal of Chemical Physics, accepted (2023).

[56] J. Algaba, I. M. Zerón, J. M. Míguez, J. Grabowska, S. Blázquez, E. Sanz, C. Vega, and F. J. Blas, "Solubility of carbon dioxide in water: Some useful results for hydrate nucleation," The Journal of Chemical Physics **158**, 054505 (2023).

[57] D. van der Spoel, E. Lindahl, B. Hess, G. Groenhof, A. E. Mark, and H. J. Berendsen, "Gromacs: Fast, flexible, and free," J. Comput. Chem. **26**, 1701–1718 (2005).

[58] U. Essmann, L. Perera, M. L. Berkowitz, T. Darden, H. Lee, and L. G. Pedersen, "A smooth particle mesh Ewald method," J. Chem. Phys. **103**, 8577–8593 (1995).

[59] L. Lundberg and O. Edholm, "Dispersion corrections to the surface tension at planar surfaces," Journal of Chemical Theory and Computation **12**, 4025–4032 (2016), pMID: 27409361, https://doi.org/10.1021/acs.jctc.6b00182.

[60] M. A. Cuendet and W. F. V. Gunsteren, "On the calculation of velocity-dependent properties in molecular dynamics simulations using the leapfrog integration algorithm," J. Chem. Phys. **127**, 184102/1–9 (2007).

[61] S. Nosé, "A molecular dynamics method for simulations in the canonical ensemble," Mol. Phys. **52**, 255–268 (1984).

[62] M. Parrinello and A. Rahman, "Polymorphic transitions in single crystals: A new molecular dynamics method," J. Appl. Phys. **52**, 7182–7190 (1981).

[63] J. Grabowska, S. Blázquez, E. Sanz, E. G. Noya, I. M. Zerón, J. Algaba, J. M. Míguez, F. J. Blas, and C. Vega, "Homogeneous nucleation rate of methane hydrate formation under experimental conditions from seeding simulations," J. Chem. Phys. (submitted).

[64] S. Blazquez, I. Zeron, M. Conde, J. Abascal, and C. Vega, "Scaled charges at work: Salting out and interfacial tension of methane with electrolyte solutions from computer simulations," Fluid Phase Equilibria **513**, 112548 (2020).

[65] P. Montero de Hijes, J. R Espinosa, C. Vega, and C. Dellago, "Minimum in the pressure dependence of the interfacial free energy between ice ih and water," The Journal of Chemical Physics **158**, 124503 (2023).

[66] S. Blazquez, M. Conde, and C. Vega, "Scaled charges for ions: An improvement but not the final word for modeling electrolytes in water," The Journal of Chemical Physics **158**, 054505 (2023).

[67] J. L. F. Abascal, E. Sanz, R. G. Fernández, and C. Vega, "A potential model for the study of ices and amorphous water: TIP4P/Ice," J. Chem. Phys. **122**, 234511–1–234511–9 (2005).

[68] M. M. Conde, M. Rovere, and P. Gallo, "High precision determination of the melting points of water TIP4P/2005 and water TIP4P/Ice models by the direct coexistence technique," J. Chem. Phys. **147**, 244506 (2017).

[69] J. J. Potoff and J. I. Siepmann, "Vapor-liquid equilibria of mixtures containing alkanes, carbon dioxide, and nitrogen," AIChE Journal. **47**, 1676–1682 (2001).

[70] B. Guillot and Y. Guissani, "A computer simulation study of the temperature dependence of the hydrophobic hydration," The Journal of Chemical Physics **99**, 8075–8094 (1993), https://pubs.aip.org/aip/jcp/article-pdf/99/10/8075/11040096/8075_1_online.pdf.

[71] D. Paschek, "Temperature dependence of the hydrophobic hydration and interaction of simple solutes: An examination of five popular water models," The Journal of Chemical Physics **120**, 6674–6690 (2004), https://pubs.aip.org/aip/jcp/article-pdf/120/14/6674/10855058/6674_1_online.pdf.

[72] E. M. Freer, M. S. Selim, and E. D. Sloan Jr, "Methane hydrate film growth kinetics," Fluid Phase Equilibria **185**, 65–75 (2001).

[73] A. Touil, D. Broseta, and A. Desmedt, "Gas hydrate crystallization in thin glass capillaries: Roles of supercooling and wettability," Langmuir **35**, 12569–12581 (2019).

[74] T. Uchida, T. Ebinuma, J. Kawabata, and H. Narita, "Microscopic observations of formation processes of clathrate-hydrate films at an interface between water and carbon dioxide," Journal of crystal growth **204**, 348–356 (1999).

[75] J. D. Wells, W. Chen, R. L. Hartman, and C. A. Koh, "Carbon dioxide hydrate in a microfluidic device: Phase boundary and crystallization kinetics measurements with micro-raman spectroscopy," The Journal of Chemical Physics **154**, 114710 (2021).

[76] H. D. Nagashima, M. Oshima, and Y. Jin, "Film-growth rates of methane hydrate on ice surfaces," Journal of Crystal Growth **537**, 125595 (2020).

[77] W. Ou, W. Lu, K. Qu, L. Geng, and I.-M. Chou, "In situ raman spectroscopic investigation of flux-controlled crystal growth under high pressure: A case study of carbon dioxide hydrate growth in aqueous solution," International Journal of Heat and Mass Transfer **101**, 834–843 (2016).

[78] D. Daniel-David, F. Guerton, C. Dicharry, J.-P. Torré, and D. Broseta, "Hydrate growth at the interface between water and pure or mixed co2/ch4 gases: Influence of pressure, temperature, gas composition and water-soluble surfactants," Chemical Engineering Science **132**, 118–127 (2015).

[79] S. Blazquez, M. M Conde, C. Vega, and E. Sanz, "Growth rate of co2 and ch4 hydrates by means of molecular dynamics simulations," The Journal of Chemical Physics **159** (2023).

[80] Y.-T. Tung, L.-J. Chen, Y.-P. Chen, and S.-T. Lin, "The growth of structure i methane hydrate from molecular dynamics simulations," The Journal of Physical Chemistry B **114**, 10804–10813 (2010).